The Effects of the Bubble size on the Bubble Dispersion and Skin Friction Reduction

Takafumi KAWAMURA*, Akiko FUJIWARA*, Takahito TAKAHASHI***,
Hiroharu KATO**, Youichiro MATSUMOTO*, Yoshiaki KODAMA***

*The University of Tokyo, JAPAN
**Toyo University, JAPAN
***National Maritime Research Institute, JAPAN

Abstract

The purpose of this study is to elucidate the effects of the bubble size on the skin friction reduction and its persistence. Various bubble injection methods were examined for controlling the bubble size. Measurements of the bubble distribution and skin friction were carried out for a spatially developing boundary layer in a test section and 50 m flat plate ship model in a towing tank. The results indicate that the small bubbles disperse faster while large bubbles stay close to the wall due to the buoyancy force. It has been also confirmed that the skin friction reduction persists for longer distance when the bubble size is large. This suggests that larger bubbles are more efficient for the purpose of skin friction reduction of a ship.

1. Introduction

Since the bubble size is supposed to be one of the most important parameters which can influence the efficiency of the microbubble drag reduction, we have devoted special efforts to the development of the injection methods for controlling the bubble size and to the experimental investigations for identifying the effect of bubble size [1, 2, 3]. But so far we have not found any evidence that the bubble size is important, while it was rather clearly shown that the drag reduction in a fully developed channel flow is independent of the bubble size when the average diameter is between 0.5 and 2.0 mm [3].

Several experimental results indirectly suggest that small bubbles are more suitable. For example, Gore and Crowe [4] have shown that solid particles decrease turbulent intensity of the carrier phase when the ratio of the particle size to the turbulence scale is smaller than unity. This suggests that small bubbles may suppress the liquid phase turbulence. On the other hand, it is supposed that small bubbles are more rapidly dispersed than large bubbles. The dispersion of bubbles leads to decrease in the near-wall void fraction and in the skin friction reduction. However, since it has been difficult to achieve sufficiently high void fraction with very small bubbles, the overall effect has not been clarified yet.

The purpose of this study is to give a conclusive answer to the question which bubble size is the most efficient for the purpose of the microbubble drag reduction. For this goal, a new bubble generator utilizing cavitation in a venturi tube was developed. By using the new bubble generator, the effect of bubble size below 0.5mm is investigated for a spatially developing boundary layer in a channel. Large scale experiments using 50 m flat plate ship were also carried out using three different bubble injection methods.

2. Bubble generators

Venturi tube type bubble generator

This bubble generator has a very simple structure as shown in Fig. 1. Air is injected at upstream side of the throat. As the mixture of the air and water passes the nozzle throat, the bubbles grow due to the pressure decreases caused by the increase in the velocity. Then the bubbles collapse in the diverging part of the nozzle because of the recovery of the pressure. Due to the decrease in the sonic speed in the bubbly flow, the flow velocity exceeds the sonic speed. This forms a shock wave in the diverging region, and the bubbles are supposed to experience very steep pressure recovery.

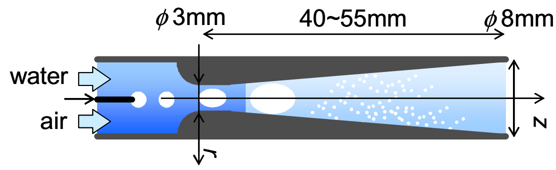

Fig. 1 Schematic sketch of the venturi tube type bubble generator

The performance of this venturi tube type bubble generator was evaluated for ranges of air volume fraction and liquid flow rate. Fig. 2 shows the relation between the void fraction α and the bubble size distribution. It is shown that bubble size distribution is quite independent of the void fraction up to $\alpha = 20\%$. The arithmetic mean diameter is about 0.1 mm. The symbol D_S in the figure denotes the area equivalent diameter defined as

$$D_s = \frac{\sum_i D_i^3}{\sum_i D_i^2} \qquad (1)$$

Fig. 3 shows that bubble size distribution changes when the liquid flow rate is small. This is due to the different collapsing behavior at a low and a high liquid flow rate. As shown in Fig. 4, at the liquid flow rate Q_w = 6.7 *l*/min bubbles collapse suddenly, while change in the diameter is slower at Q_w = 4.2 *l*/min. The simple average velocity V at the throat is 9.9 m/s at Q_w = 4.2 *l*/min, and 15.8 m/s at Q_w = 6.7 *l*/min. The corresponding cavitation number $\sigma = (P_\infty - P_v)/0.5\rho V^2$ is about 2.0 and 0.80 respectively. It is supposed that the intensive collapse of bubbles occur when cavitation number $\sigma < 1.0$.

This venturi tube type bubble generator is used in the channel experiment shown in Section 3 for investigating effect of small bubbles.

Porous Plate (PP), Array-of-Holes Plate (AHP), Slit Plate (SP)

For the experiment using the 50 m flat plate ship, bubbles were generated by injecting air through three different bubble generator plates mounted flush with the ship bottom. The width, length and the thickness of the plates are 500 mm, 100 mm, and 4 mm, respectively. PP is made of sintered bronze of which the nominal grain size is 2μm. AHP has a total of 3300 holes of 1 mm in diameter. The holes are arranged staggered at the interval of 3 mm in the spanwise direction and 5 mm in the streamwise direction. SP has one slit of 5.2 mm wide and 500 mm long. The total orifice areas of AHP and SP are the same. Fig. 5 shows the photographs of the three bubble generator plates.

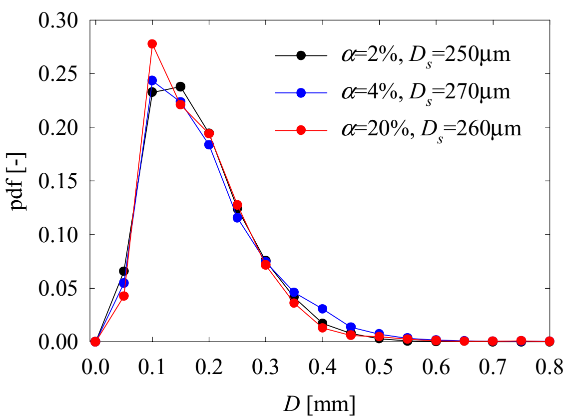

Fig. 2 Bubble size distribution at different void fractions (Venturi tube microbubble generator, liquid flow rate Q_w=5.3 *l*/min)

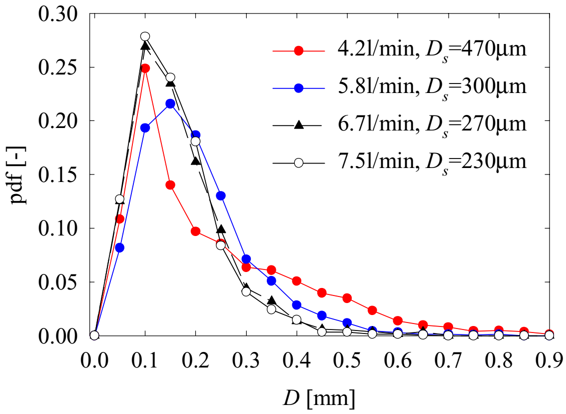

Fig. 3 Bubble size distribution at different liquid flow rates Q_w (Venturi tube microbubble generator, void fraction α=4%)

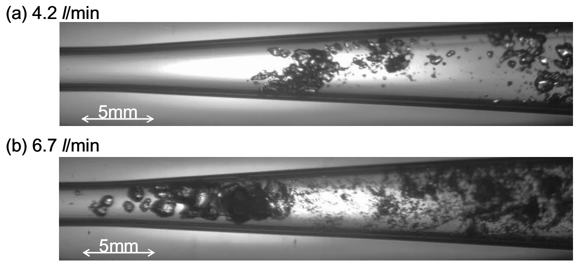

Fig. 4 Collapse of bubbles in the venturi tube type bubble generator at low and high liquid flow rates

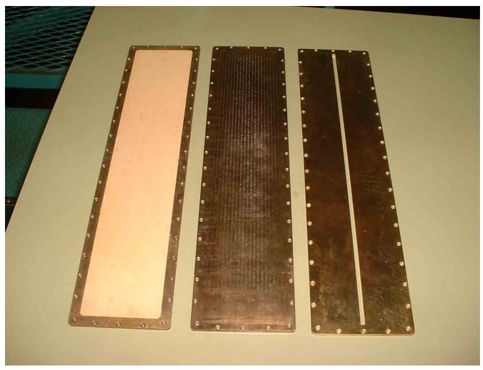

Fig. 5 Air injection plates used with 50m flat plate ship (left: PP, middle: AHP, right: SP)

3. Channel experiment

Experimental setup

Fig. 6 shows the setup of the experiment carried out at the University of Tokyo. The test section is 120 mm high and 50 mm wide. The air and water are mixed in the bubble generator and introduced into the test section through 8 mm wide slit which occupies the whole 50 mm width. In this paper, the results for the main flow velocity of 4.0 m/s are shown. The boundary layer thickness at the slit is about 10 mm, and is developing through the test section. 50 ppm of 3-pentanol is added as surfactant to suppress coalescence of bubbles. It was confirmed in a preliminary examination that the mean bubble diameter did not change

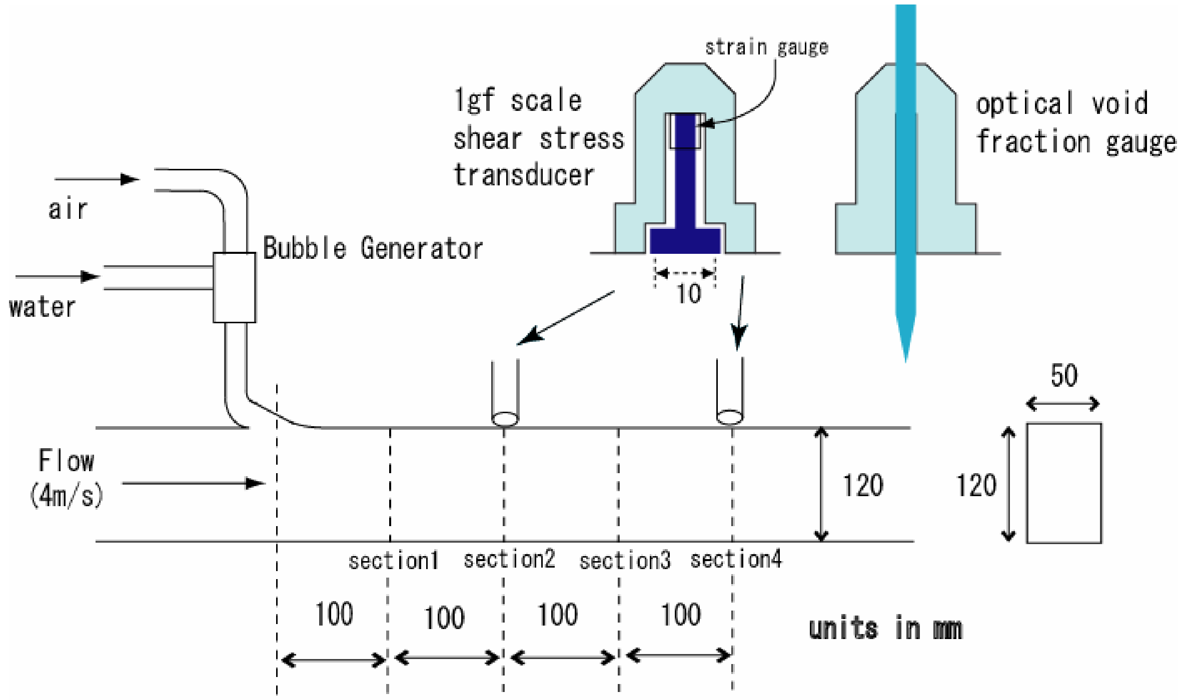

Fig. 6 Setup of the channel flow experiment

significantly in the test section. The local shear stress was measured by floating disk type shear stress transducers mounted flush with the top wall at positions 200, 400 and 700 mm downstream from the injection slit (referred to as Section 2, 4, and 7 respectively). For the measurement of the local void fraction, the shear stress transducer was replaced with a fiber optical void fraction gauge.

Three different bubble generators shown in Fig. 7 were used for generating bubbles of different sizes. The straight tube type generator is used for making large bubbles. It is similar to the venturi tube type generator, but the difference is that the inner diameter is constant. The decompression type generator is different from the other two in that air is not pumped in but dissolved in water under a high pressure. In this study, water is sufficiently aerated under the gauge pressure of 0.7 MPa and introduced into the test section in which the gauge pressure is zero. The pressure drop occurs at the valve shown in the figure, and the excess air is separated as very fine microbubbles [1]. The bubbly mixture of water and air is introduced into the test section through the 8 mm wide slit. The flow near the injection slit was examined by CFD simulation using a commercial CFD code Fluent 6.1. It was confirmed that the injected bubbly flow smoothly mixes with the main flow without any flow separation or recirculation as shown in Fig. 8.

Bubble size

Fig. 9 compares the bubbles generated by the three bubble generators. The bubble size distribution obtained from the photographs is shown in Fig. 10. The bubbles generated by the straight tube type generator are quite large and the distribution is quite dispersed. The photograph shows that those large bubbles are strongly deformed. On the other hand, bubbles generated by the venturi tube type generator are mono-dispersed. Most bubbles are less than 0.4 mm in diameter. The photograph indicates the bubbles are almost spherical. The bubbles generated by the decompression type generator are very small and it is difficult to identify single bubbles from Fig. 9 (c). Note that only exceptionally large bubbles are visible in Fig. 9 (c), and the small bubbles appear as white cloud. The arithmetic mean diameter D is 1.4, 0.4 and 0.04 mm for the straight tube type, the venturi tube type, and the decompression type bubble generators respectively. Although the decompression type generator can generate very fine microbubbles, it is not very useful because the void fraction is limited and it is difficult to control the air flow rate. Therefore we mainly compare the other two bubble generators in this paper.

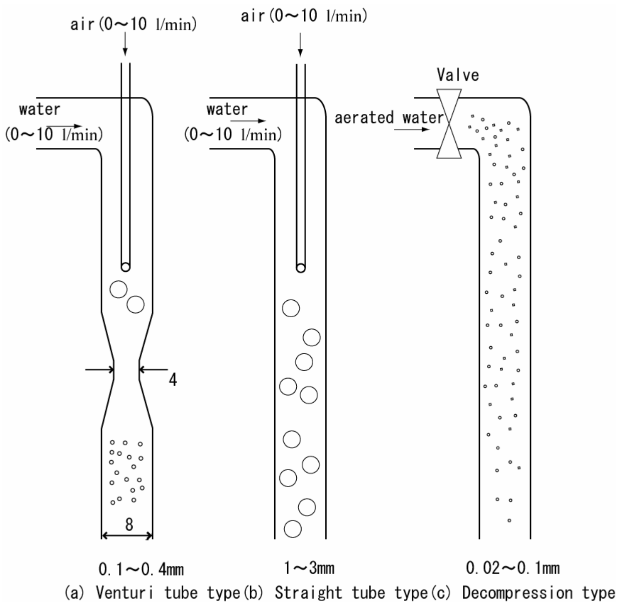

Fig. 7 Three types of bubble generators used in the channel experiment

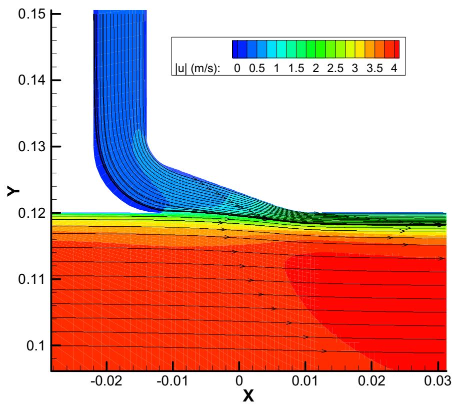

Fig. 8 Flow near the injection slit computed by a commercial CFD code Fluent 6.1.

Bubble dispersion

It was found that the bubble size strongly influences the void fraction profile. Fig. 11 shows photographs of bubbles taken from side wall of the channel at Section 4. Small bubbles from the venturi tube type generator in Fig. 11 (b) are more widely distributed than large bubbles from the straight tube type generator shown in Fig. 11 (a). This difference is also confirmed in the void fraction profiles measured by the optical void fraction gauge shown in Fig. 12. It is clearly shown that the large bubbles from the straight tube type generator are more concentrated near the wall and that the profiles at Section 2 and at Section 4 are almost the same. On the other hand, the small bubbles from the venturi tube type generator are more dispersed already at Section 2, and spreads further at the downstream sections.

This difference is explained by turbulent dispersion of bubbles. The void fraction profiles take the maximum values at about 3 mm away from the wall and decrease rapidly toward the wall and more gradually towards the direction away from the wall. As shown in Fig. 13, it is assumed that the dominant forces acting on bubbles in the region far from the wall are the buoyancy force F_B and the turbulent diffusion force F_D, while in the near wall region the wall effect is assumed to be significant. The buoyancy force per unit bubble volume is

$$F_B = \rho_l g \,, \tag{2}$$

in which ρ is density and g is gravitational acceleration, and the subscript l denotes the liquid phase. According to Drew [5], the diffusion force is estimated to be

$$F_D = -C_{TD} \frac{\rho_l k_l}{S_t} \frac{\nabla \alpha}{\alpha} \,, \tag{3}$$

where C_{TD} is the model constant, k is turbulent kinetic energy, α is void fraction, and S_t is the Stokes number defined as

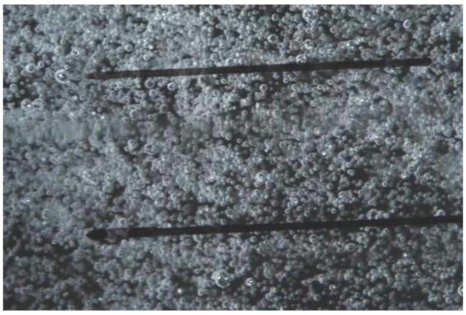
(a) Venturi tube type

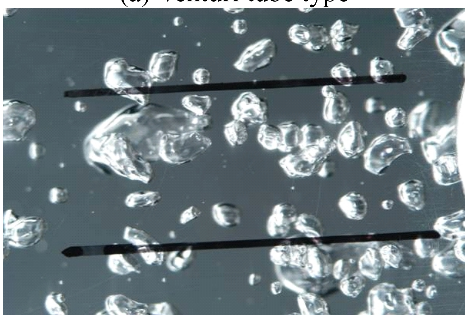
(b) Straight tube type

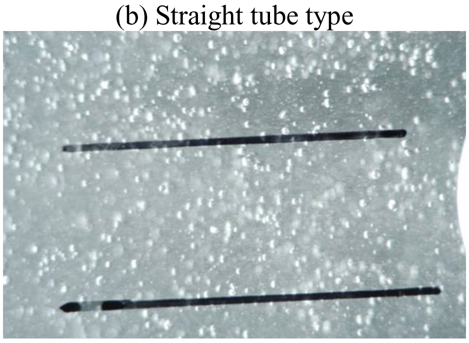
(c) Decompression type

Fig. 9 Comparison of bubbles generated by the three bubble generators seen from the top. The distance between the two lines is 10mm (Q_a=4 l/min, Q_w= 10 l/min)

$$S_t = \frac{D^2 \varepsilon_l}{18 \nu_l k_l} \quad (4)$$

with ε being the dissipation rate. Then the ratio of the diffusion force to the buoyancy force is estimated to be,

$$\frac{F_D}{F_B} \propto \frac{\rho_l k_l \nabla \alpha}{S_t \rho_l g \alpha} \propto \frac{U^2}{gLS_t} = \frac{F_d^2}{S_t} \quad (5)$$

where U and L are the representative velocity and length scale respectively, and F_d is the Froude number. This means that the bubble dispersion can be scaled by the non-dimensional parameter F_d^2/S_t. It is also predicted that the equilibrium void fraction gradient in the region far from the wall is scaled as

$$\frac{\nabla \alpha}{\alpha} \propto \frac{gS_t}{k} \propto \frac{gD^2 \varepsilon}{\nu k_l^2} \propto \frac{gD^2}{\nu \nu_t} \quad (6)$$

where ν_t is the turbulent viscosity. The equation

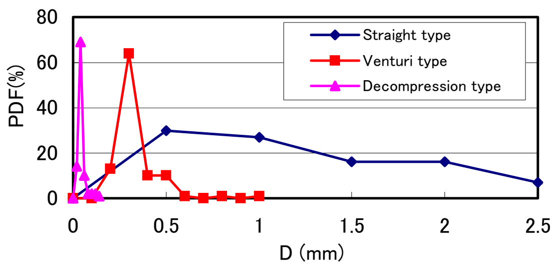

Fig. 10 Comparison of the bubble size distribution in the channel

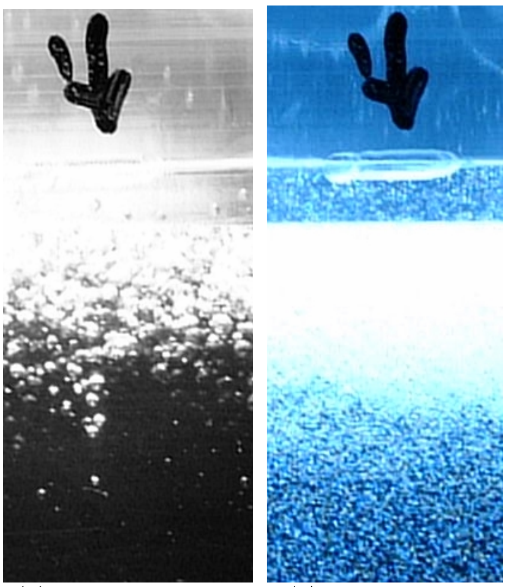

(a) Straight-type (D=1.4mm) (b) Venturi-type (D=0.3mm)

Fig. 11 Photographs of bubbles taken from side wall of the channel at Section 4 (400 mm downstream from the injection slit) Ql = 10 l/min, Qa=4l /min

(6) predicts the void fraction gradient at D = 1.4 mm is 22 times larger than at D = 0.3 mm, while the ratio from the present experimental result is from about 10 to 13.

Guin et al [6] have shown that the skin friction reduction is correlated to the void fraction near the wall. The present result suggests that the skin friction reduction effect is larger when the mean bubble size is larger. This is confirmed by the direct measurement of the shear stress in this experiment.

Skin friction reduction

The measurement of the shear stress was carried out at Section 2, 4 and 7. The measured shear stress normalized by the shear stress without air injection is shown in Fig. 14. At Section 2 and 4, the skin friction reduction rate seems to be independent of the bubble generators used, while at Section 7 the reduction rate with the venturi tube type generator is smaller when Q_a is small. This is probably explained by the decrease of the void fraction near the wall due to the bubble dispersion. Although it was not quantitatively measured, the average bubble size of the venturi tube type generator increased with increasing air flow rate Q_a. The recovery of the skin friction reduction at high Q_a is probably due to the increase in the average bubble size.

Moriguchi & Kato [3] concluded that the skin friction reduction does not depend on the bubble size when the average diameter is larger than 0.5 mm. However, the present results indicate that the overall efficiency of the microbubble skin friction reduction can decrease due to bubble dispersion if the average bubble size is about 0.3 mm. Moriguchi & Kato's conclusion is based on the measurements of a fully developed bubbly boundary layer flow in a narrow channel, while a spatially developing boundary layer was used in this study. It is probably concluded that the effect of the bubble size is significant in the transient flow and when the average bubble size is sufficiently small.

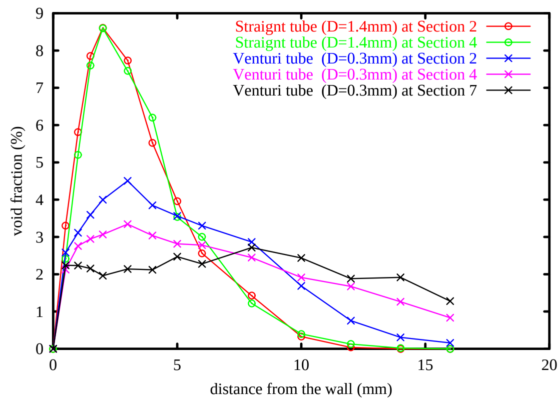

Fig. 12 Comparison of the local void fraction profiles measured by the optical void fraction gauge (Q_a=4 l/min, Q_w= 10 l/min)

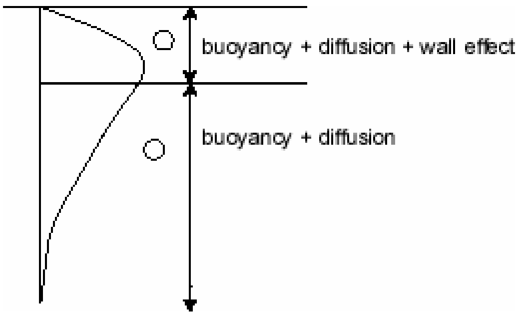

Fig. 13 Schematic sketch of the distribution of forces acting on bubbles

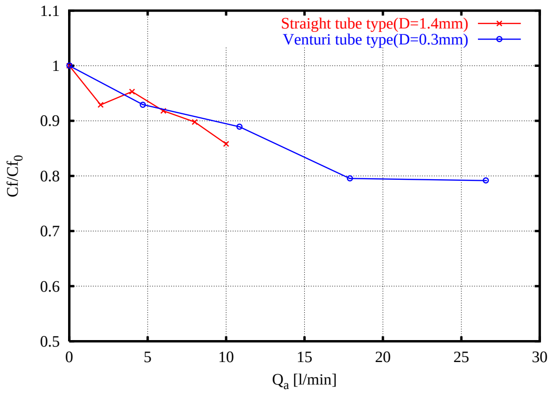

(a) Section 2 (200 mm from the injection slit)

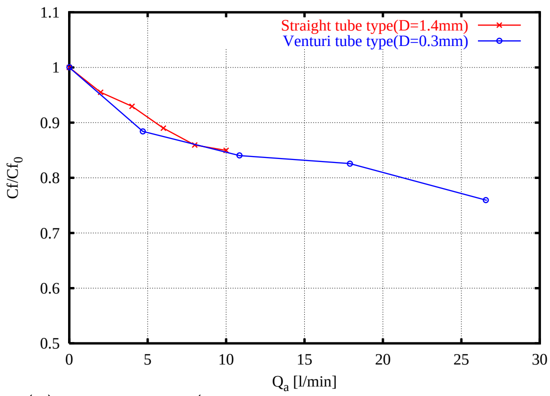

(b) Section 4 (400 mm from the injection slit)

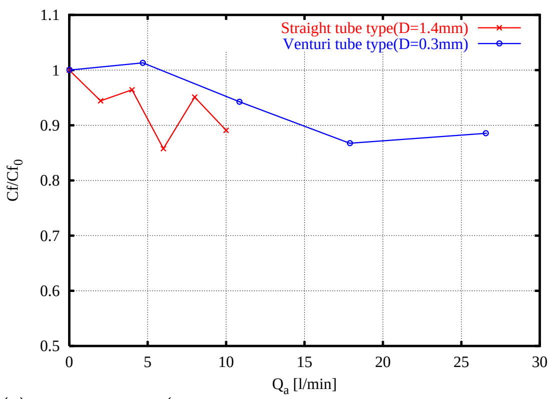

(c) Section 7 (700 mm from the injection slit)

Fig. 14 Comparison of the measured shear stress in the channel flow experiment

4. 50 m flat plate ship model

Fig. 15 shows the plan view of the 50 m flat plate ship model. The experiment using this ship model was carried out in the 400 m long towing tank of the National Maritime Research Institute. The three different bubble generators described in Section 2 were used. Fig. 16 shows the measured total resistance R_t normalized by that without bubble injection R_{t0} at the towing speed of V=5 m/s and V=7 m/s. The abscissa of the figure is the apparent air layer thickness t_a defined as $t_a = Q_a / BV$ with Q_a and B being the air flow rate and the width of the injection area respectively. The results indicate that the drag reduction rate does not significantly depend on the injection method used. This is probably because the bubble size is determined by the flow property of the boundary layer and rather independent of the injection method. However, it is clearly shown that the drag reduction rate is higher at V=5 m/s than at V=7 m/s. According to the channel flow experiment, the buoyancy force more effectively suppresses the bubble dispersion at a slower towing speed, or at a smaller Froude number. This result confirms this assumption.

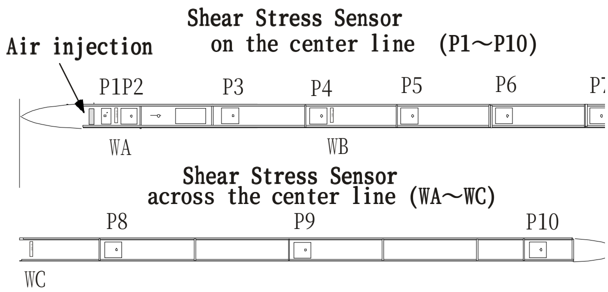

Fig. 15 Plan view of the 50 m flat plate ship model

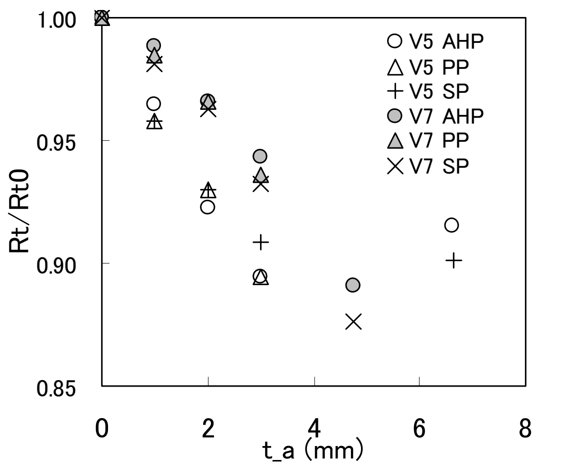

Fig. 16 Total skin friction reduction of the 50m flat plate ship model versus the apparent air layer thickness t_a.

5. Conclusion

The effects of the bubble size on the bubble dispersion and the skin friction reduction have been studied experimentally. The main conclusion is that small bubbles possibly decrease the overall efficiency of the microbubble drag reduction through dispersion. This effect of the bubble size on the dispersion is significant when the average bubble diameter is smaller than 0.5 mm, and in the spatially developing boundary layer. This result suggest that a simple bubble generator such as the slit plate (SP) used in the experiment using 50 m flat plate ship model is suitable in practical implementation because of the relatively large bubble size and small pressure loss.

Acknowledgement

The authors would like to thank Mr. Satoshi Motoyama, Mr. Jin Sakamoto of Toyo University, and Mr. Masatsugu Maeda and Masaru Miyanaga of the University of Tokyo for carrying out the experiment.

References

[1] Kawamura, T., Kakugawa, A., Kodama, Y., Moriguchi, Y., Kato, H., (2003), “Controlling the Size of Microbubbles for Drag Reduction,” Proceedings of the 3rd Symposium on Smart Control of Turbulence, University of Tokyo, Tokyo, Japan, March 4-6, (2002), pp. 121-128

[2] Kitagawa, A., Fujiwara, A., Hishida, K., Kakugawa, A., Kodama, Y., (2003), “Turbulence structures of microbubble flow measured by PIV/PTV and LIF techniques”, Proceedings of the 3rd Symposium on Smart Control of Turbulence, University of Tokyo, Tokyo, Japan, March 2-4, (2003), pp. 131-140

[3] Moriguchi, Y., and Kato, H. (2002), “Influence of microbubble diameter and distribution on frictional resistance reduction”, J. Marine Science and Technology, Vol.7 No.2, pp. 79 – 85

[4] Gore, R. A., and Crowe, C. T. (1989) “Effect of particle size on modulating turbulent intensity,” Intern J Multiphase Flow, Vol. 15, No. 2, pp. 279-285

[5] Drew, D. A., (2001), “A turbulent dispersion model for particles or bubbles,” Journal of Engineering Mathematics vol. 41, pp. 259-274

[6] Guin M. M., Kato, H., Yamaguchi, H., Maeda, M., and Miyanaga, M., (1996), “Reduction of skin friction by microbubbles and its relation with near-wall bubble concentration in a channel,” J. Marine Science and Technology, vol. 1, pp. 241-254